Int. J. Electrochem. Sci., 11 **(2016)** 10581 – 10591, doi: 10.20964/2016.12.13

International Journal of
ELECTROCHEMICAL
SCIENCE
www.electrochemsci.org

Preparation of Nano-$Ag_4Bi_2O_5$ with Co-precipitation Method and Study of Its Application for Oxygen Reduction Reaction

Dongmei Chen[1], *Pingyuan Wang*[2], *Xun Zeng*[2], *Yanzhi Sun*[2], *Bixue Zhu*[1,*], *Junqing Pan*[2,*]

[1] Key Laboratory of Macrocyclic and Supramolecular Chemistry，Guizhou University，Guiyang 550025, P.R. China
[2] State Key Laboratory of Chemical Resource Engineering, Beijing University of Chemical Technology, Beijing 100029, P.R. China
[*]E-mail: bxzhu@gzu.edu.cn ; jqpan@mail.buct.edu.cn

Received: 22 July 2016 / *Accepted:* 26 September 2016 / *Published:* 10 November 2016

Nano $Ag_4Bi_2O_5$ rods were synthesized by co-precipitation method, in which mixed $AgNO_3$- $Bi(NO_3)_3$ solution was used as Ag-Bi source and KOH solution as precipitant. The structure, morphology and composition were researched via powder X-ray diffraction (XRD), X-ray photoelectron spectroscopy (XPS) and scanning electron microscope (SEM), etc. Results show that the $Ag_4Bi_2O_5$ were nanorods crystal with 20-30 nm in width and 200-300 nm in length. Electrochemical measurements indicate that the $Ag_4Bi_2O_5$ has excellent performance for oxygen reduction reaction (ORR) followed a four-electron transfer pathway in alkaline electrolyte. Moreover, $Ag_4Bi_2O_5$ was further tested in an assembled zinc-oxygen (Zn-O_2) battery, which discharged up to 1400 h at 10 mA cm^{-2}. So essentially, the inexpensive and available $Ag_4Bi_2O_5$ electrocatalyst has superior electro-catalytic activity and good durability.

Keywords: Co-Precipitation; $Ag_4Bi_2O_5$; Electrocatalysis

1. INTRODUCTION

Fuel cell is an electrochemical device which can convert chemical energy to electrical energy efficiently with environment friendlyness [1-2]. Hydrogen oxidation reaction（HOR）and oxygen reduction reaction(ORR) are usually catalyzed by noble metals such as platinum in fuel cells due to its low exchange current density [3-7]. In comparison, ORR's low exchange current density of 10^{-9} A cm^{-2} on the cathode, while HOR's is reach 10^{-3} A cm^{-2} which is far higher than ORR's. For the hydrogen-oxygen fuel cells, even though the current density on Pt based catalyst has reaches 2 A cm^{-2}, the overpotential of hydrogen electrode is no more than 50 mV. However the overpotential of the oxygen electrode can reach 300~400mV even if the current density is very low. So more noble metals such as

Pt, an expensive metal that is not abundant, have been carried as the cathode catalyst [8]. To reduce the cost of catalyst, many researchers have devoted to develop a new, efficient, and non-platinum series catalysts as cathode oxygen reduction catalyst. Among these non-precious metal catalysts in the present study, including a transition metal composite oxides (spinel-type perovskite, pyrochlore type, etc) [9-12], transition metal sulfides [13-14], and other transition metals-contaning compunds in the carbon-nitrogen material (M-N_x-C) [15-18], etc.

Herein, the prepared $Ag_4Bi_2O_5$ is reported as a new efficient electrocatalyst for ORR in alkaline electrolyte. The $Ag_4Bi_2O_5$ nano rods with 20-30 nm in width and 200-300 nm in length was obtained by the co-precipitation method and examined by SEM and TEM. The catalyst shows superior electrochemical performances of ORR activity and durability by CV, RDE and discharge tests. This enhancement might benefit from the synergetic effects among Ag and Bi.

2. EXPERIMENT

2.1 Materials

The following reagents were used to prepare various solutions: Silver oxide (99.7%, Tianjin Fuchen Industry), and Bismuth oxide (99% Tianjin Fuchen Industry), Potassium hydroxide (95% Chengdu Huarong Chemical Co., Ltd), Nitrate (65~68% Beijing Chemical Plant), and Manganese dioxide (EMD) (Jianchen Electrolytic Manganese Industry Company), Pt/C (20 wt.%) was purchased from Shanghai River Electric Co., Ltd. All chemical reagents were analytically pure and did not get any further treatment.

2.2 Preparation of $Ag_4Bi_2O_5$

A schematic diagram describing the catalyst synthesis is shown in scheme 1. The $Ag_4Bi_2O_5$ was synthesized by co-precipitation method as followed: 1.16 g Ag_2O and 1.17 g Bi_2O_3 were dissolved in 50 mL 1 mol L^{-1} HNO_3 as Ag-Bi source. 38.38 g KOH was dissolved into deionized water to obtain 100 mL 6.5 mol L^{-1} KOH as precipitant. 50 mL salt solution was pumped into the base solution at 30^{o}C at a flow rate of 3 mL min^{-1}, with the strong agitating of 2000 rpm. In Scheme 1, it can be seen that the sample will be obtained as amorphous at the end of co-precipitation. After crystallization for 30 minutes, it turns to a mixture of amorphous and crystalline. After crystallization for 60 minutes, it turns into complete crystal. Then, the filtrate was washed with deionized water until the solution became neutral. At last, the product was dried in vacuum at 30^{o}C for 24 hours. The reaction equation is as follows:

$$4AgNO_3+2Bi(NO_3)_3+10KOH=Ag_4Bi_2O_5\downarrow+10KNO_3+5H_2O$$

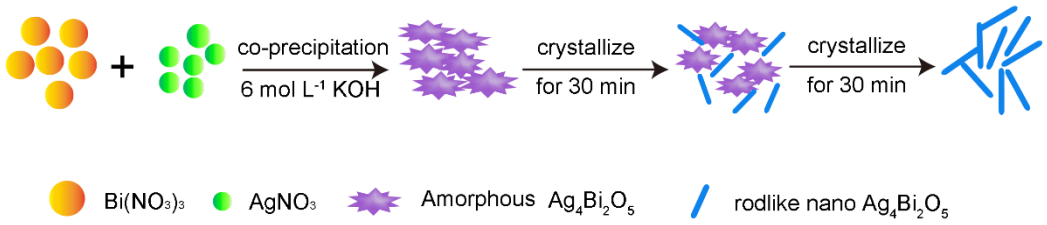

Scheme 1. Schematic representation of the preparation procedure for the $Ag_4Bi_2O_5$

2.3 Electrochemical measurement of the *$Ag_4Bi_2O_5$ oxygen cathode*

The rotating disk electrode (RDE, PINE AFMSRCE) tests were carried out with a three-electrode system at 25°C. The catalyst inks were prepared by adding 5 mg catalyst ($Ag_4Bi_2O_5$), 32 mg conductive graphite (Timcal-ks6 Timical), 330 μL isopropanol solution (99.5%, Beijing Chemical Plant), 670 μL deionized water, and 50μL Nafion (5 wt.%, D520 DuPont). After a ultrasonic treatment under a sonication (KQ-100DB，Kunshan ultrasonic instruments Co. Ltd.) process for 30 min. 10 μL of the catalyst ink was taken by a TopPette Pipettor (0.5–10μL, Eppendorf Research) and dropped onto the glassy carbon rotating disk electrode (φ = 8 mm, Pine Instrument). The saturated calomel electrode (SCE) was used as a reference electrode, a platinum wire as the auxiliary electrode. Before the RDE voltammetry experiments for ORR, the solution was saturated by O_2 or Ar gas.

To further investigate electrochemical activity and stability of the catalysts, we carried out the cyclic voltammetry (CV) measurements in ultra-high purity argon or oxygen-saturated 0.1 mol L^{-1} KOH solution at room temperature. Electrochemical impedance spectroscopy (EIS) spectra was tested with the frequency range from 1 to 2 × 10^6 Hz. An electrochemical workstation (Shanghai Chen Hua, CHI760D) was used for to obtain CV and EIS.

The preparation of $Ag_4Bi_2O_5$ oxygen electrode is similar to the literature [19].

The prepared oxygen electrode was used as working electrode, SCE electrode was used as reference electrode and nickel sheets were used as the auxiliary electrode. The discharge property of the assembled zinc-oxygen (Zn-O_2) battery was tested by LAND cell test system (CT2001, Wuhan LAND Electronics Co., Ltd.) in 9 mol L^{-1} KOH electrolyte solution.

2.4 Structural and Morphological characterizations

The powder X-ray diffraction (XRD) patterns of the prepared $Ag_4Bi_2O_5$ were obtained by a Rigaku D/max2500VB2+/PCX X-ray diffractometer with a Cu Kα anticathode (40 kV, 200 mA) at a scanning rate of 10^o min^{-1} and a scanning angle (2θ) from 10^o to 90^o. The scanning electron microscope (SEM, ZEISS, SUPRA 55), a transmission electron microscope (TEM, Hitachi, H-800) and a high resolution transmission electron microscope (HR-TEM, JEOL JEM-2100F) were used to examine the morphology of the synthesized samples, X Energy Dispersive X-Ray Spectroscopy (EDS&EDX) spectrum analysis was carried out on a X-ray energy instrument (LINK-ISIS300, Oxford). The chemical state of element was analyzed by X-ray photoelectron spectroscopy (XPS) on a

ULVAC- PHI Quantera SXM. The thermal stability of catalysts was monitored by TG-DTA (STA 449F 3A) with a heating rate of 10^{o}C min^{-1} from 20^{o}C to 800^{o}C in N_2 atmosphere.

3. RESULTS AND DISCUSSION

3.1 Structural characterization of the prepared samples

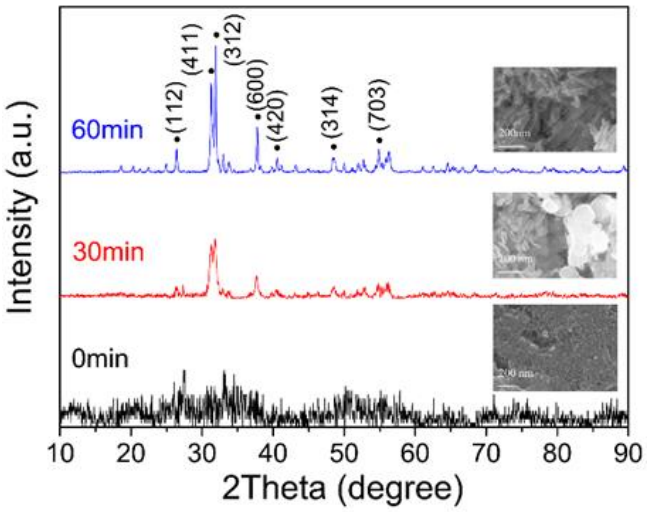

Figure 1. The XRD pattern and corresponding SEM pictures of $Ag_4Bi_2O_5$

The structure and morphology of $Ag_4Bi_2O_5$ were examined by the XRD patterns and SEM pictures in Fig. 1. We can see that the sample obtained at the end of the reaction is amorphous.

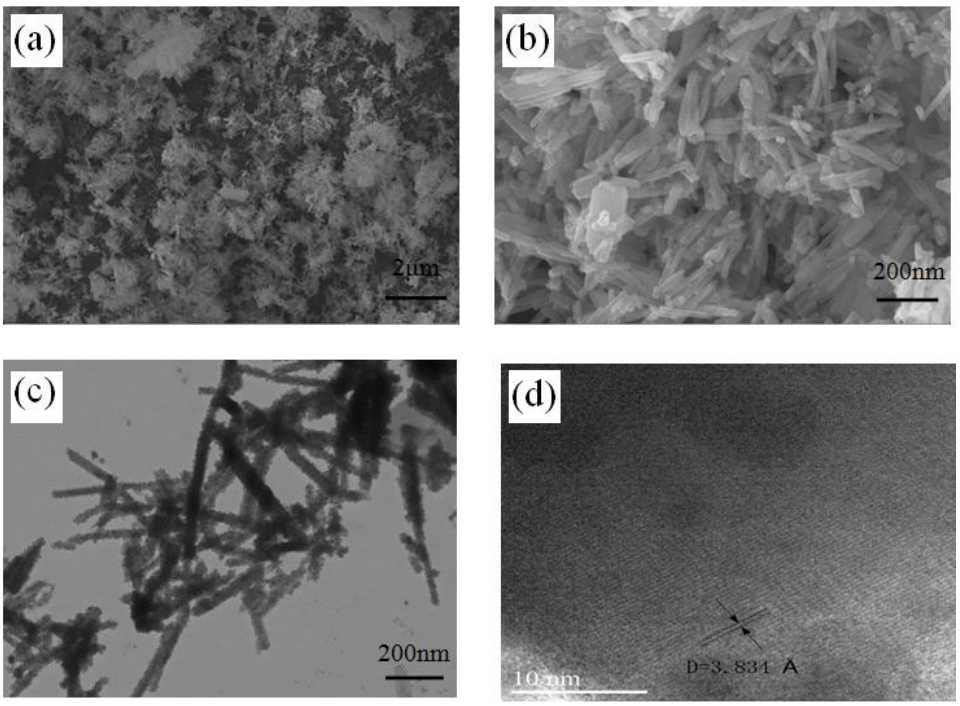

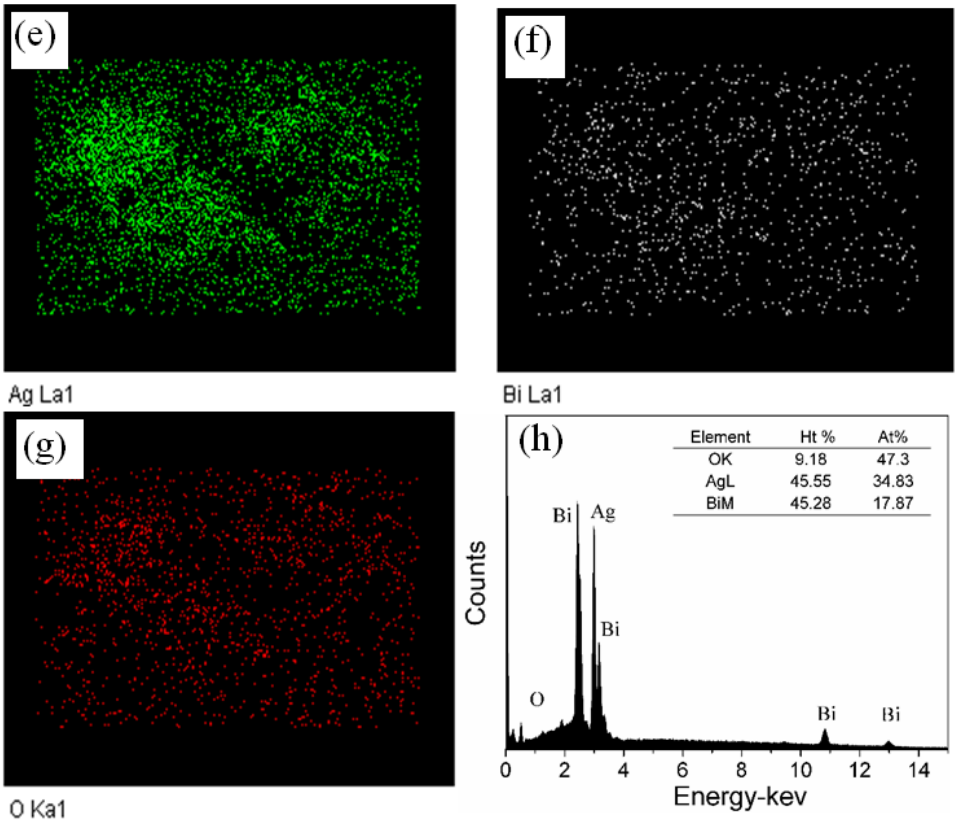

Figure 2. SEM (a, b), TEM (c), HR-TEM (d), The EDX elemental mapping images (e, f, g), and EDS spectrum of the $Ag_4Bi_2O_5$ sample.

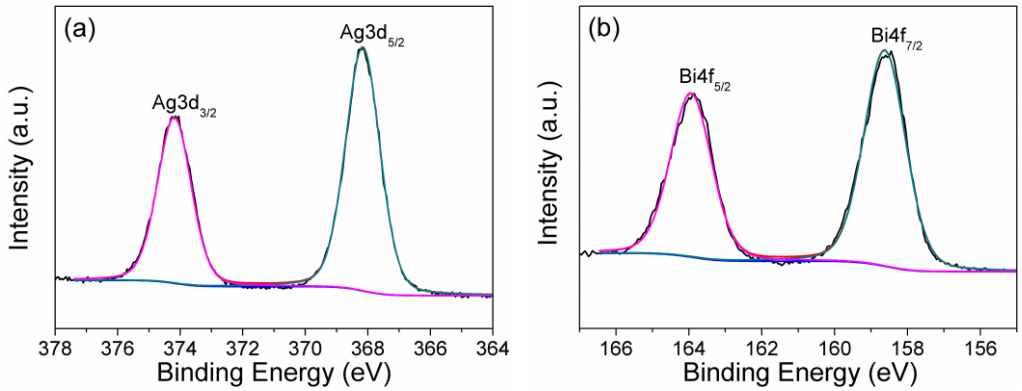

Figure 3. XPS spectra of the $Ag_4Bi_2O_5$ sample(a) Ag 3d and (b) Bi 4f

After crystallization for 30 minutes, it turns into a mixture of amorphous and crystalline. After crystallization for 60 minutes, it turns to complete crystal. It is shown that the $Ag_4Bi_2O_5$ sample has six strong peaks at 26.37°, 31.25°, 31.85°, 37.76°, 40.50°, 48.35° and 54.81°, corresponding to the (112), (411), (312), (600), (420), (314) and (703) facets of the structure of $Ag_4Bi_2O_5$ (JCPDS 87-0866), respectively [20]. The particle size was calculated by the Scherrer formula $D_{hkl}=0.89\lambda/B\cos\theta$. For example, the integral half width FWHM of (411) crystal line is 0.322, 2θ is 31.30°, λ is 0.154056 nm, therefore, the crystal size of the sample is 25.35 nm. The particle size of $Ag_4Bi_2O_5$ is much smaller than that of the sample prepared previously by our research group.

Fig. 2a and Fig. 2b show the SEM images of the $Ag_4Bi_2O_5$ sample, which indicates as-prepared catalyst is a nano rod with 20-30 nm in width and 200-300 nm in length. This SEM examination is well consistent with the calculation result of XRD, as confirmed by TEM images in Fig 2c. Fig. 2d shows the HR-TEM image of the $Ag_4Bi_2O_5$ catalyst. The spacing of the lattice fringes is 0.3834 nm, corresponding well to the (211) planes of $Ag_4Bi_2O_5$. EDX and EDS analysis were also performed (Fig 2e, 2f, 2g and 2h) to get the chemical composition of the catalyst. Besides the peak of oxygen, the peaks of metal elements Ag and Bi are displayed clearly. Fortunately, the atomic ratio of Ag:Bi:O was 34.83: 17.87: 47.30, conforming to the atomic ratio 4:2:5 in the $Ag_4Bi_2O_5$.

The XPS spectrum of $Ag_4Bi_2O_5$ sample (Fig.3) further confirms the chemical state of Ag and Bi elements. XPS spectrum of the Ag 3d signal of catalyst is showed in Fig. 3a, the band observed at 368.18 and 374.17 eV is assigned to the Ag $3d_{5/2}$ and Ag $3d_{3/2}$ of Ag(Ⅰ)$_2$O. As seen from Fig. 3b, the typical Bi $4f_{7/2}$ and $4f_{5/2}$ at 158.63 eV and 163.92 eV can be attributed to the peaks of Bi(Ⅲ)$_2O_3$ [21].

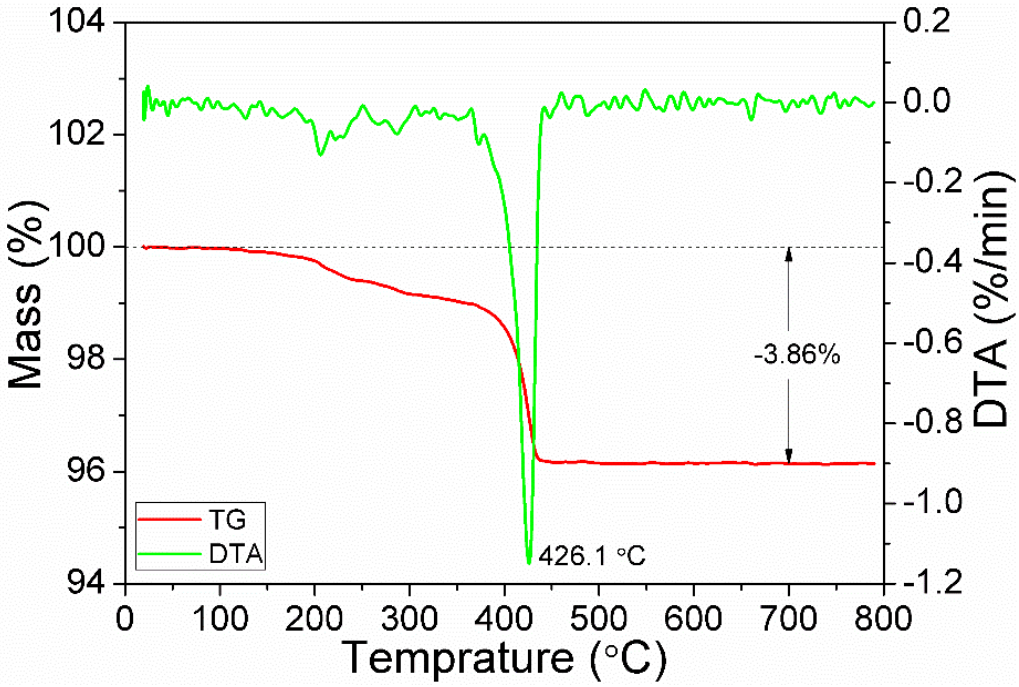

Figure 4. The TG-DTA curves of the $Ag_4Bi_2O_5$ sample

The thermal gravimetric curves and temperature dependence of gas evolution are tested by TG-DTA measurements. Which are showed in Fig. 4, it can be clearly seen that an endothermic peak appears at 426.1^{o}C, the possible reaction equation is described as follows:

$Ag_4Bi_2O_5 \rightarrow 4Ag + Bi_2O_3 + O_2\uparrow$

Theoretical weight loss rate is calculated to be 3.11%, while the observed total weight loss is 3.86%, which are approximately to each other. From Fig. 4, we can see that the catalyst is stable at room temperature. From 20^{o}C to 380^{o}C, 1% weight loss of the sample may be adsorbed on the surface of trace moisture. When the temperature reaches 380^{o}C, the oxygen evolution reaction takes place and

the catalyst are decomposed into silver and bismuth oxide, which is according to the reports basically [20].

3.2 Electrochemical characterization and enhancement meachanims

The cyclic voltammograms (CVs) of ORR on the as-prepared $Ag_4Bi_2O_5$ in Ar and O_2-saturated 0.1 mol L^{-1} KOH solution are shown in Fig. 5. It was seen that a strong peak positioned at -0.26 V (vs. SCE) in the existence of O_2 ambiance, however, no significant peak at the same potential in Ar atmosphere (Fig. 5a). It was clear that the oxygen reduction reaction occurs on the surface of the catalyst. So there is an oxygen reduction reaction occurring on the surface of the catalyst. Fig. 5b shows the reduction curve of catalyst keeps almost unchanged after 1000 cycles, confirming that the catalyst is stable [19]. The catalyst has good reversibility with the oxidation peak increases synchronously with enhanced scan rate of 5 mv s^{-1} to 100 mv s^{-1} (Fig. 5c). In addition, we can see that the peak currents are linear to the square root of the scan rate, as shown in Fig. 5d.

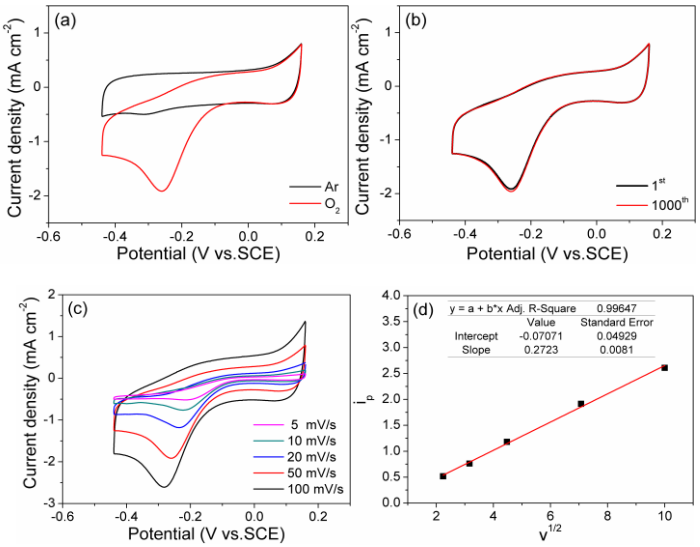

Figure 5. (a) CV of $Ag_4Bi_2O_5$ electrode at scan rate of 50 mV s^{-1} in a 0.1 mol L^{-1} KOH solutions saturated with Ar and O_2, (b) CV of $Ag_4Bi_2O_5$ before and after 1000 cycles, (c) CV of $Ag_4Bi_2O_5$ electrode at different scan rates, and (d) The peak current as a function of the scan rate

The electrocatalytic activities of as-synthesized $Ag_4Bi_2O_5$ for the ORRwas performed in electrolyte (0.1 mol L^{-1} KOH) with O_2 and Ar-saturated at a scan rate of 5 mV s^{-1}, as shown in Fig. 6a. Seven curves substantially coincide at higher potential E> -0.3V. The oxygen reduction reaction is slower, and the speed of rotating disk electrode has little effect on the reaction, indicating that the ORR catalyst process of oxygen (O_2) on glassy carbon electrode surface is controlled by an electrochemical process at high potential. At lower potential E <-0.3V, it was observed that the cathodic reduction current is related to the solubility of oxygen in solution. With the increasing of the rotating speed of the RDE electrode, the diffusion layer of dissolved oxygen on the surface of the rotating disk electrode

gradually decrease. The results revealed a linear relationship between the update rates and the exchange current density of oxygen on the catalyst surface. We can see that at high polarization potential, the oxygen reduction current density and speed also present linear relationship, which indicates that the oxygen reduction current density is controlled by the liquid phase diffusion of oxygen at potential from -0.6 V to -0.3 V.

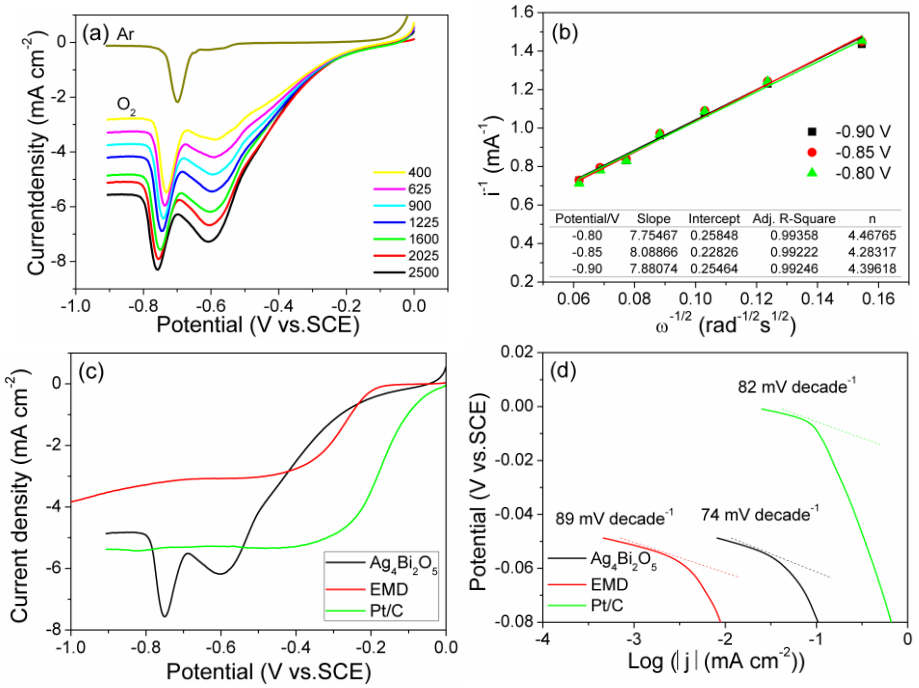

Figure 6. (a) The rotating disk test for $Ag_4Bi_2O_5$ catalyst at different rotating rates, (b) the K-L plots for $Ag_4Bi_2O_5$ at different potentials, (c) LSV of the $Ag_4Bi_2O_5$, EMD and Pt/C, and (d) Tafel slope of the $Ag_4Bi_2O_5$, EMD and Pt/C.

Furthermore, a strong peak at -0.77V is the reduction peak of Bi(Ⅲ)→Bi(0) of $Ag_4Bi_2O_5$ by combining with the scanning experiments at argon (Ar) atmosphere [19]. The number n of electron transfer in oxygen reduction process can be calculated according to the Koutechy–Levich (K-L) formalism as given by [22,23]: $i^{-1}=B+1/K\times1/(\omega^{1/2})$, in which $K=0.62nFC_0D^{2/3}\nu^{-1/6}$, where i is the current density, ω is the electrode rotating rate, n is the overall number of electrons transferred in ORR, F is the Faraday constant of 96485 C mol^{-1}, C_0 is the bulk concentration of O_2 (1.26×10^{-3} mol L^{-1}), D is the diffusion coefficient of O_2 in 0.1 mol L^{-1} KOH (1.93×10^{-5} cm^2 s^{-1}) and ν is the kinetic viscosity (0.01 cm^2 s^{-1}). The parameter K at different applied voltages could be obtained from the slope of the $-i^{-1}\sim\omega^{-1/2}$ plots in Fig. 6b. The relationship of all curves at different potentials is approximately linear and the slopes are almost the same. In the scanning potential −0.8 V, −0.85 V, −0.9 V, the electron transfer number is 4.4, 4.2, and 4.3, respectively as shown in Fig. 6b. The LSV of EMD, $Ag_4Bi_2O_5$ and Pt/C catalyst was investigated in Fig. 6c. In contrast, $Ag_4Bi_2O_5$ catalyst exhibited good activity similar to Pt/C catalyst under the same condition. The Tafel slope of EMD, $Ag_4Bi_2O_5$ and Pt/C is 89, 74 and 82mV per decade (Fig. 6d). The low ORR Tafel slope of $Ag_4Bi_2O_5$ implies a transition from

Langmuirian adsorption to the Temkin adsorption of adsorbed O/OH groups [22]. Therefore, the electrochemical catalyst activation of $Ag_4Bi_2O_5$ is superior to EMD and close to that of Pt/C.

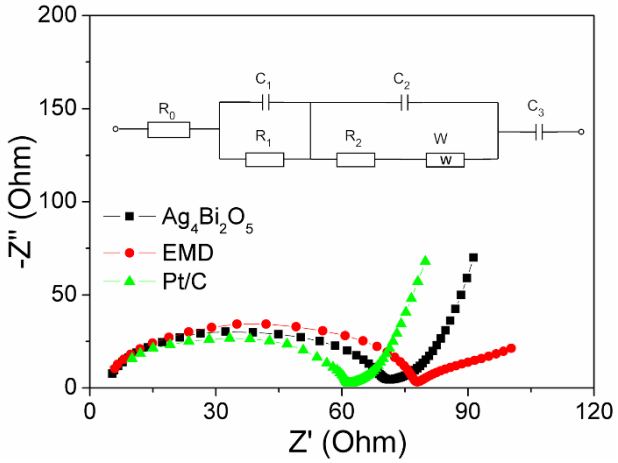

Figure 7. EIS spectra of the $Ag_4Bi_2O_5$, EMD and Pt/C samples

The impedance spectra of the $Ag_4Bi_2O_5$, EMD and Pt/C are consisted of one semicircle and a slope, as shown in Fig. 7. Where inset shows the equivalent circuit of the three electrodes, R_0, R_1, R_2 are represented as solution resistance, adsorption resistance and electrochemical reaction resistance, C_1, C_2 and C_3 are denoted as adsorption capacitance, W refers to Warburg impedance. A nonlinear, least-square fitting calculation is done with the above equivalent circuit [24]. In table 1, for $Ag_4Bi_2O_5$ electrode, the R_2 and C_2 value (T) are 5.14 Ω g and 7.814×10^{-6} F g^{-1}, EMD electrode are 15.16 Ω g and 3.892×10^{-5} F g^{-1}, and Pt/C electrode 3.043 Ω g and 1.403×10^{-5} F g^{-1}. The value of R_2 of the $Ag_4Bi_2O_5$ electrode is smaller than that of the EMD but greater than that of Pt/C electrodes, in accordance well with the CVs and polarization curves. The value of C_2 has something to do with the true reaction areas of the electrode. Therefore, for the value of double layer capacitance of $Ag_4Bi_2O_5$ electrode is greater than that of the EMD and Pt/C electrodes, this means that the $Ag_4Bi_2O_5$ electrode has more enormous true reaction area [25].

Table 1. The equivalent circuit fitting parameters of the $Ag_4Bi_2O_5$, EMD and Pt/C samples

Name	R_0(Ω g)	R_1(Ω g)	R_2(Ω g)	C_1(F g^{-1})	C_2(F g^{-1})	C_3(F g^{-1})	W(Ω^{-1})
$Ag_4Bi_2O_5$	4.597	63.33	5.14	2.368E-8	7.814E-6	2.147E4	3.832E3
EMD	4.446	73.67	15.16	1.915E-8	3.892E-5	6.64E4	3.973E3
Pt/C	5.428	55.21	3.043	1.095E-8	1.403E-5	2.136E4	4.449E3

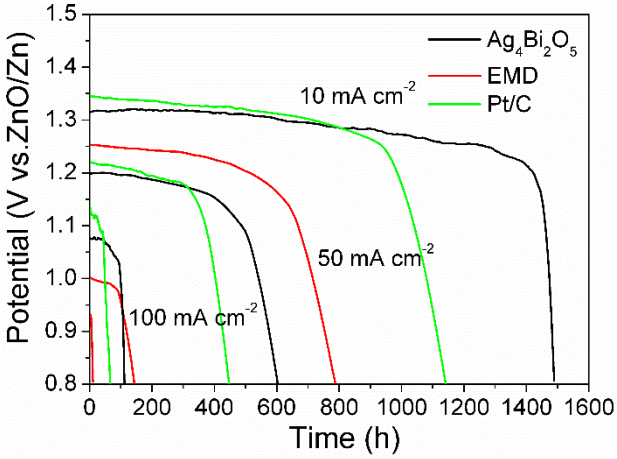

Figure 8. Discharge curves of EMD, $Ag_4Bi_2O_5$ and Pt/C catalyst at different current densities.

The discharge testing for EMD, $Ag_4Bi_2O_5$ and Pt/C oxygen electrode was carried out at different current densities. As shown in Fig. 8, the $Ag_4Bi_2O_5$ electrode exhibits a superior oxygen electrode life of 1400h than EMD and Pt/C at the current density of 10 mA cm^{-2}. $Ag_4Bi_2O_5$ electrode exhibits similar discharge voltage and discharge time to that of Pt/C at the current density of 50 mA cm^{-2} while EMD presents poorly elechochemical property. $Ag_4Bi_2O_5$ electrode exhibits much higher discharge voltage and longer discharge time than EMD at the current density of 100 mA cm^{-2}.

4. CONCLUSION

Nano $Ag_4Bi_2O_5$ was synthesized by co-precipitation method successfully. XRD and SEM show that the sample is a nano rod with 20-30 nm in width and 200-300 nm in length. The RDE demonstrate that $Ag_4Bi_2O_5$ has excellent electrocatalytic activity towards ORR in alkaline electrolyte. The discharge test indicates that $Ag_4Bi_2O_5$ electrode has long discharge life at a constant current density showing ORR has good oxygen reduction activity and durability.

ACKNOWLEDGEMENTS
The authors are thankful for the State Key Program of National Natural Science of China (21236003), National Natural Science Foundation of China (21476022), BUCT Fund for Disciplines Construction and Development (XK1531), and the Fundamental Research Funds for the Central Universities (JD1515 & YS1406).

References

1. B. C. H. Steele, A. Heinzel, *Nature*, 414 (2001) 345.
2. Y. Yu, H. Li, H. Wang, X. Z. Yuan, G. Wang, and M. Pan, *J. Power Sources*, 205 (2012) 10.
3. P. Costamagna, S. Srinivasan, *J. Power Sources*,102 (2001) 242.
4. Y. J. Li, C. C. Chang, T. C. Wen, *J. Appl. Electrochem*, 27 (1997) 227.

5. D. Banham, S. Y. Ye, K. T. Pei, J. I. Ozaki, T. Kishimoto and Y. Imashiro, *J. Power Sources,* 285 (2015) 334.
6. A. Schenk, C. Grimmer, M. Perchthaler, S. Weinberger, B. Pichler, C. Heinzl, C. Scheu, F. A. Mautner ,B. Bitschnau and V. Hacker, *J. Power Sources,* 266 (2014) 313.
7. G. Diloyan, M. Sobel, K. Das and P. Hutapea, *J. Power Sources*, 214 (2012) 59.
8. W. Li, Z. Chen, L. Xu and Y. Yan, *J. Power Sources*, 195 (2010) 2534.
9. R. Ding, L. Qi, M. J. Jia, H. G. Wang, *Nanoscale,* 6 (2014) 1369.
10. H. C. Bo, S. A. Park, B. K. Park, H. H. Chun and Y. T. Kim, *Materials Research Bulletin*, 48 (2013) 3651.
11. T. Hyodo, M. Hayashi, N. Miura and N. Yamazoe, *J. Electrochem. Soc.* 143 (1996) L266.
12. H. Kawai, K. Yoshihara, T. Konishi, M. Saito, J. Kuwano and H. Shiroishi, *Key Engineering Materials*, 421 (2010) 479.
13. A. Lewera, J. Inukai, W. P. Zhou, D. Cao, H. T. Duong, N. Alonso-Vante, A. Wieckowski, *Electrochim. Acta*, 52 (2007) 5759.
14. Z. Zheng, N. Li, C. Q. Wang, D. Y. Li, F. Y. Meng, Y. M. Zhu and Q. Li, *J. Power Sources*, 230 (2013) 10.
15. .L. C. Wang, L. Zhang and J. J. Zhang, *Electrochim. Acta,* 56 (2011) 5488.
16. G.Wu, K. L. More, C. M. Johnston and P. Zelenay, *Science*, 332 (2011) 443.
17. Domínguez, C., Pérez-Alonso F. J., S. A. Al-Thabaiti, S. N. Basahel, A. O. Alyoubi, A. A. Alshehri, M. A. Pena and S. Rojas, *J. Power Sources,* 271 (2014) 87.
18. J. H. Lee, M. J. Park, S. J. Yoo, J. H. Jang, H. J. Kim, S. W. Nam, C. W. Yoon and J. Y. Kim, *Nanoscale,* 7 (2015) 10334.
19. Y. Z. Sun, M. Yang, J. Q. Pan, P. Y. Wang, W. Li, P. Y. Wan, *Electrochim. Acta*, 197 (2016) 68.
20. J. Q. Pan, Q. Wang, Y. Z. Sun and Z. H. Wang, *Electrochim. Acta*, 59 (2012) 515.
21. C. D. Wagner, A. V. Naumkin, A. Kraut-vass, J. W. Allison, C. J. Powell, J. R. Rumble, NIST X-ray Photoelectron Spectroscopy Database (Version 3.5). http://srdata.nist.gov/xps.
22. F. W. T. Goha, Z. L. Liu, X. M. Ge, Y. Zong, G. J. Du and T. S. A. Hora, *Electrochim. Acta,* 114 (2013) 598.
23. F. P. Hu, X. G. Zhang, F. Xiao and J. L. Zhang, *Carbon*, 43 (2005) 2931.
24. H. L. Gao, Z. Y. Li, X. Qin, *J. Power Sources*, 248(2014) 565.
25. S. W. Liu, X. Qin, *RSC. Adv.*, 5 (2015) 15627.